

Spectral properties of the non-hermitian Wilson-Dirac operator in the Schrödinger functional

HU-EP-07/45
SFB/CPP-07-60

Shinji Takeda, Oliver Witzel* and Ulli Wolff

Humboldt Universität zu Berlin, Institut für Physik, Newtonstr. 15, 12489 Berlin, Germany

E-mail: witzel@physik.hu-berlin.de

We report on some preparatory investigations for the simulation of the QCD Schrödinger functional with a non-hermitian polynomial hybrid Monte Carlo algorithm. The complex spectrum of the non-hermitean free operator with SF boundary conditions is computed semianalytically. Then it is shown how one can obtain relevant information on the boundary of the spectral domain also in the presence of nontrivial gaugefields by monitoring the behavior of polynomials in the Wilson operator applied on random vectors.

*The XXV International Symposium on Lattice Field Theory
July 30 - August 4 2007
Regensburg, Germany*

*Speaker.

1. Introduction

Inverting the Wilson-Dirac operator is one of the dominant costs in simulating lattice QCD with dynamical fermions. A possibility to avoid the explicit inversion is to replace it by a polynomial approximation of the inverse Wilson-Dirac operator.[1, 2] This allows moreover for a deviation from importance sampling with the Boltzmann factor to be compensated by reweighting, which can be useful. In addition simulations with odd numbers of flavors become possible. Our focus here is the approximate inversion of the non-hermitian Wilson-Dirac operator. According to reference [3] the approximation of the non-hermitian operator is supposed to be superior to the hermitian version. Each approximation depends on the typical spectrum of the operator to be approximated. Therefore, we here report about some spectral properties of the Wilson-Dirac operator with respect to Schrödinger Functional(SF)[4] boundary conditions (BC) and investigate how they affect the polynomial approximation.

2. Computing the spectrum semianalytically

In the hopping parameter representation Wilson's fermion action [5] reads

$$S_f = \sum_{xy} \bar{\psi}(x) [\delta_{xy} - \kappa H_{xy}] \psi(y), \quad (2.1)$$

and the Wilson-Dirac operator is defined by $M_{xy} = \delta_{xy} - \kappa H_{xy}$, where the nearest neighbor interaction is carried by the hopping operator

$$H_{xy} = \sum_{\mu=0}^3 \left(U_{\mu}(x)(1 - \gamma_{\mu})\delta_{x+\hat{\mu},y} + U_{\mu}^{\dagger}(y)(1 + \gamma_{\mu})\delta_{x-\hat{\mu},y} \right). \quad (2.2)$$

Important spectral features of H depend on the boundary conditions. In general H is not normal i.e. $[H, H^{\dagger}] \neq 0$.

In order to get a first idea of the spectrum and to develop methods for the general case we start by computing the eigenvalues of H in the free case i.e. $U_{\mu} \equiv 1$ in the SF with vanishing background field. Since translation invariance in the spatial directions still holds we set

$$\psi(x) = \psi(x_0) \cdot e^{i\vec{p}\vec{x}}. \quad (2.3)$$

using plain waves for the space dependence. This ansatz leads to a reduced 1-dimensional operator of the form

$$E = \frac{1 - \gamma_0}{2} h_0 + \frac{1 + \gamma_0}{2} h_0^{\dagger} + i\gamma_1 \alpha, \quad \alpha^2 = \sum_{k=1}^3 \sin^2(p_k) \quad (2.4)$$

acting on ψ_0 . In (2.4) h_0 is the 1-dimensional hopping operator given for the SF by the nilpotent matrix

$$h_0 = \begin{pmatrix} 0 & 1 & 0 & \dots & 0 \\ 0 & 0 & \ddots & & \vdots \\ \vdots & & \ddots & & \vdots \\ 0 & & \dots & 1 & 0 \\ 0 & & \dots & 0 & 1 \\ 0 & & & \dots & 0 & 0 \end{pmatrix}. \quad (2.5)$$

By itself it has only one $(T - 1)$ fold degenerate zero eigenvalue. The matrix E is related to H by

$$\text{spec}(H) = 2\text{spec}(E) + 2 \sum_{k=1}^3 \cos(p_k). \quad (2.6)$$

Finding the eigenvalues of E is equivalent to locating the zeros of a smaller determinant

$$0 = \det \left[\lambda_0^2 + \lambda_0 (\mathbf{h}_0 + \mathbf{h}_0^\dagger) + \mathbf{h}_0^\dagger \mathbf{h}_0 + \alpha^2 \right]. \quad (2.7)$$

We could not obtain them in closed form, but approximations are possible. Here we simply compute the eigenvalues of E numerically for some range of α .

These eigenvalues are shown in Fig. 1 together with the corresponding ones for (anti)periodic boundary conditions that follow trivially from Fourier expansion. For small α the latter approach the value 1 leading to zeromodes in $1 - \kappa_c H$ (up to lattice artefacts for antiperiodic BC), where κ_c equals $1/8$. In the SF we see that the eigenvalues are ‘deflected’ away from unity. For very small α one can show the behavior

$$|\lambda_0| \propto \alpha^{1/T} \quad \text{as} \quad \alpha \rightarrow 0. \quad (2.8)$$

This is how a gap of order $1/T$ is maintained in the SF (even in the continuum limit).

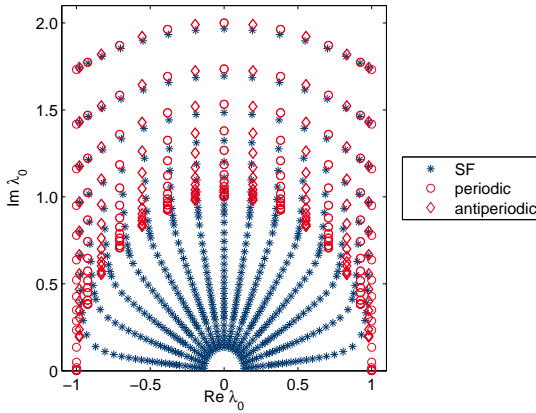


Figure 1: Numerical spectrum of E for $T = 16$ and $\alpha^2 = \text{tiny} \dots 3$.

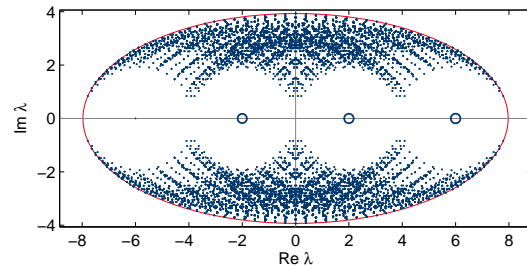


Figure 2: Spectrum of the hopping operator H on a 16^4 lattice with $U_\mu \equiv \mathbb{1}$ and SF boundary conditions.

We conclude this subsection by showing in Fig. 2 a complete spectrum of H computed numerically. An ellipse with major half axis $a = 7.971$, minor half axis $b = 3.932$ and eccentricity $e = \sqrt{a^2 - b^2} = 6.933$ is drawn that obviously describes the spectral boundary very well. In the centers of the void areas there are (degenerate) eigenvalues for which α vanishes due to the zero mode of h_0 . Roundoff errors in the eigenvalue routine in combination with the behavior (2.8) ‘inflate’ three of these dots to small circles.

3. Approximation of the inverse Wilson-Dirac operator

To start simple we first approximate the inverse Wilson-Dirac operator by a geometric series

$$M^{-1} \approx P_n^G(M) = \sum_{j=0}^n (\kappa H)^j = \frac{1 - (\kappa H)^{n+1}}{1 - (\kappa H)}, \quad \text{for } \|\kappa H\| < 1, \quad (3.1)$$

and define the remainder

$$R_{n+1} = \mathbb{1} - MP_n^G(M) = (\kappa H)^{n+1}. \quad (3.2)$$

By construction R_{n+1} is a small quantity and vanishes in the limit of $n \rightarrow \infty$. Moreover, it allows for a recursive implementation and its convergence can be easily monitored by computing $\|R_{n+1}\eta\|$, where η is a Gaussian random vector normalized to 1. Approximating M^{-1} by a geometric series requires a circular bound on the spectrum of radius $r = \kappa|\lambda_{\max}(H)| < 1$.¹ From the spectral radius r follows the rate of convergence

$$\mu^G(\kappa) = -\ln(\kappa|\lambda_{\max}(H)|). \quad (3.3)$$

As we have seen in the previous section the shape of the spectrum is elliptical. This fact can be exploited to improve our approximation. Expressing the remainder R_{n+1} in terms of scaled and translated Chebyshev polynomials T_n [6] we can derive an improved, recursive description, where only the eccentricity e as elliptical parameter enters

$$R_{n+1}(M) = \frac{T_{n+1}((\kappa H)/e)}{T_{n+1}(1/e)} = a_n \kappa H R_n(M) + (1 - a_n) R_{n-1}(M) \quad (3.4)$$

with $R_1(M) = \kappa H$; $R_0(M) = 1$; $a_n = (1 - a_{n-1} e^2/4)^{-1}$ and $a_1 = (1 - e^2/2)^{-1}$. The second equality in (3.4) follows from the recurrence relation of the Chebyshev Polynomials, $T_{n+1}(z) = 2zT_n(z) - T_{n-1}(z)$. By virtue of the defining relation for the remainder we obtain also a recursive expression for the Chebyshev approximation of M^{-1}

$$P_n^C(M) = a_n(1 + \kappa H P_{n-1}(M)) + (1 - a_n) P_{n-2}(M) \quad (3.5)$$

with $P_1(M) = a_1(1 + \kappa H)$ and $P_0(M) = 1$. The rate of convergence in the limit of $n \rightarrow \infty$ follows using the identity $T_n(z) = \cosh(n \operatorname{arcosh}(z))$ and by replacing κH by its eigenvalues (cf. footnote 1) [7]. The rate μ^C depends on the elliptical parameters a and e which themselves are proportional to κ

$$\mu^C(a, e) = \ln \left(\frac{1 + \sqrt{1 - e^2}}{a + \sqrt{a^2 - e^2}} \right). \quad (3.6)$$

For periodic BC the extent of the ellipse is known in the free case ($a = 8\kappa$, $e = \sqrt{48}\kappa$) and thus μ^C becomes a function of κ only, $\mu^C(\kappa) = \ln \left((1 + \sqrt{1 - 48\kappa^2}) / (12\kappa) \right)$, and vanishes like (3.3) for $\kappa \rightarrow \kappa_c$.

¹For non-diagonalizable matrices the same behavior is true asymptotically. This can be shown with the help of the Schur-decomposition.

4. Numerical results

To test our approximations numerically we monitor the norm of the remainder as a function of n and determine the convergence rate from the exponential decay. We perform this test choosing $n = 400$ and varying e to obtain a scan over the eccentricity. In Fig. 3 the results are presented for various lattice sizes.

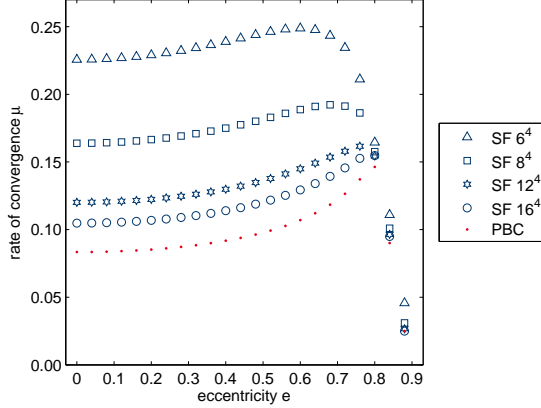


Figure 3: Rate of convergence μ as function of the eccentricity e . $U_\mu \equiv \mathbb{1}$, $\kappa = 0.115$ and each point is determined after $n = 400$ iterations.

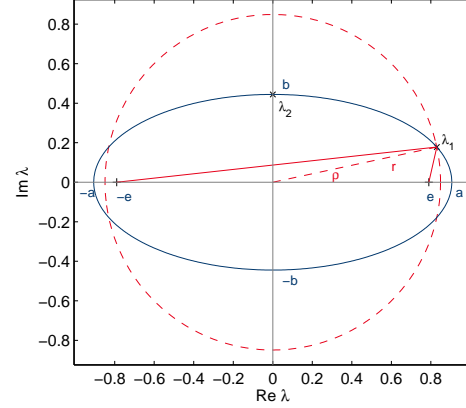


Figure 4: Sketch how to get a good guess on the eccentricity starting from the largest eigenvalues.

Obviously, there is a dependence on the lattice size in the case of the Schrödinger functional and for larger lattices the rate of convergence approaches the value corresponding to periodic BC which is independent of L (red dots in Fig. 3). Since the rate of convergence increases roughly by a factor 2 from a circular bound ($e = 0$, geometric series) to the optimal eccentricity, it is important to find this optimal value. Therefore we look again at the spectrum of the Wilson-Dirac operator and focus our attention especially on the eigenvalue λ_1 with largest real part and λ_2 with largest imaginary part of H as indicated in Fig. 4 (multiplied by $\kappa = 0.115$).

One way to obtain a guess on the eccentricity e is to use the norm of λ_2 as value for the minor half axis b . We are then seeking the ellipse which also passes through λ_1 . By the parameter form of an ellipse, $x = a \cos \rho$; $y = b \sin \rho$, and using $x + iy = \lambda_1$ we find the major half axis

$$a = \text{Re}\{\lambda_1\} / \cos(\rho) \quad \text{with} \quad \rho = \arcsin(\text{Im}\{\lambda_1\}/b). \quad (4.1)$$

Thus we can determine $e = \sqrt{a^2 - b^2}$. Beside yielding a guess on e we can moreover obtain an estimate on μ^C by eq. (3.6) in this way.

There exist different methods to determine e . In practice we are seeking a good guess on e such that the convergence rate is high and its determination is easy. These properties hopefully carry over when including a non-trivial gauge field. There we hope to find an eccentricity that changes only weakly between different gauge fields at fixed β and κ .

For a first experiment with a non-trivial gauge field we start by generating 50 pure-gauge configurations on an 8^4 lattice at $\beta = 6.0$ employing a Cabbibo-Marinari update [8]. Reading these

configuration with MATLAB (version 7.3) and using its implementation of the Arnoldi algorithm we try to compute λ_1 and λ_2 on each configuration. Unfortunately, the algorithm converged only on a subset of the configurations. Hence the mean values presented in Tab. 1 are just a rough estimation and within the quoted errors no dependence on the configuration is seen.

	U_μ	κ	r	μ^G	a	b	e	μ^C
SF	$\mathbb{1}$	0.115	0.8489	0.1638	0.9060	0.4444	0.7895	0.1781
SF	$\beta = 6.0$	0.135	0.838(4)	0.1770(7)	0.843(5)	0.47(1)	0.701(7)	0.268(3)
P	$\mathbb{1}$	0.115	0.9200	0.0834	0.9200	0.4600	0.7967	0.1506
P	$\beta = 6.0$	0.135	0.865(5)	0.1456(8)	0.869(6)	0.48(1)	0.725(2)	0.226(9)

Table 1: Expected values for μ and e derived from measured maximal eigenvalues. SF Schrödinger functional, P periodic boundary conditions.

The results indicate that the spectrum of H for non-trivial gauge fields is expected to be “rounder” and enclosed in an elliptical disc of smaller area than the one of the trivial gauge field. We check our expectation by computing the polynomial remainder using the above determined e in case of the Chebyshev approximation. While for the trivial gauge field we find perfect agreement of both methods, the differences in the rate of convergence are larger for non-trivial gauge fields when using Chebyshev polynomials

	μ^G	e	μ^C
SF	0.1776(3)	0.701	0.2127(2)
P	0.1482(4)	0.725	0.1914(2)

Table 2: Computing the convergence from the remainder test as a measure on the “integrated spectrum”.

To get a better understanding of this situation we computed for one SF configuration 800 eigenvalues with largest/smallest real part and 400 eigenvalues with largest/smallest imaginary part again using MATLAB. Figure 5 shows these data points in blue and the solid red line is the ellipse ($e = 0.701$, $a = 0.843$) derived from the eigenvalue computation. The predicted value for μ_C disagrees because the shape of the spectral boundary is not elliptical. The circular bound is still estimated correctly as can be seen by the dotted black circle with radius $r = 0.838$. Hence μ^G is in agreement. To illustrate our approximation using Chebyshev polynomials we note that by specifying e a family of confocal ellipses is determined. From this family the ellipse of smallest extent which encloses *all* eigenvalues specifies a and b , which enter into (3.6). Hence the dashed red ellipse in Fig. 5 represents better the one corresponding to the Chebyshev approximation. Here $a = 0.872$ and we compute $\mu^C = 0.208$.

Increasing a to 0.857 and b to 0.547 we yield a different ellipse ($e = 0.660$) shown with dash-dotted green line. This one encloses the computed spectrum even better and leads to the prediction $\mu^C(e = 0.660) \approx 0.221$. Taking this smaller value of e as input for the Chebyshev approximation we find for the rate of convergence $\mu^C = 0.2207(2)$ confirming the predicted value.

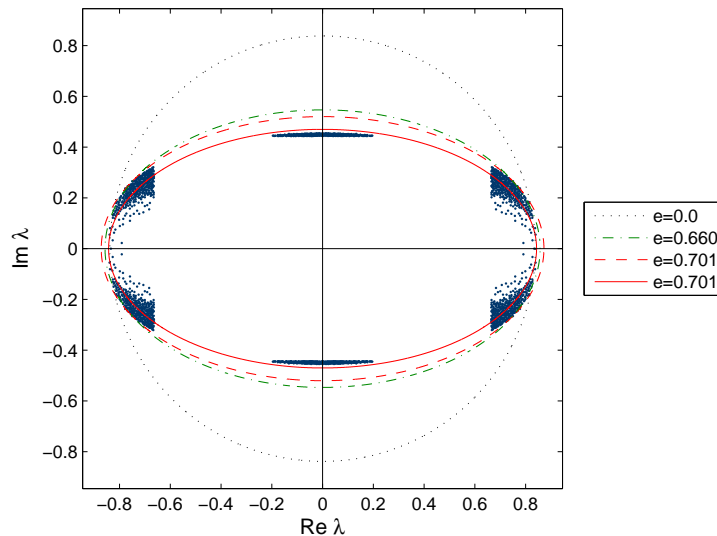


Figure 5: Computing 2400 eigenvalues of κH on one gauge configuration at $\beta = 6.0$ and $\kappa = 0.135$ with SF boundary conditions.

5. Conclusion and outlook

These preliminary studies show that a good understanding of the structure of the spectrum seems to be important to implement an algorithm approximating the inverse Wilson-Dirac operator with good performance. Moreover, useful information on how to tune such an algorithm is obtained.

Probably, the deviation of the spectrum in the SF from an elliptic disk is an artefact of small lattice sizes. A check with e.g. a 12^4 lattice would be desirable but seems to be numerically challenging. Moreover we like to study the effect of $O(a)$ improvement (Sheikholeslami-Wohlert term) and the effects of preconditioning.

Acknowledgement

This work is supported by the DFG within the SFB/TR 9 “Computational Particle Physics”.

References

- [1] Ph. de Forcrand and T. Takaishi, *Nucl. Phys. Proc. Suppl.* 53(1997) 968
- [2] R. Frezzotti and K. Jansen, *Phys. Lett. B* 402 (1997) 328
- [3] A. Borelli, Ph. de Forcrand and A. Galli, *Nucl. Phys. B* 477 (1996) 809
- [4] M. Lüscher, R. Narayanan, P. Weisz and U. Wolff, *Nucl. Phys. B* 384 (1992) 168
- [5] K.G. Wilson, *Phys. Rev. D* 10 (1974) 2445
- [6] T.A. Manteuffel, *Numer. Math.* 28 (1977) 307
- [7] B. Bunk, *Internal Notes* (1997)
- [8] N. Cabibbo and E. Marinari, *Phys. Lett. B* 119 (1982) 387